Kinetic energy analysis of O(P-3(0)) and O-2(b(1)Sigma(+)(g)) fragments produced by photolysis of ozone in the Huggins bands

Kinetic energy analysis of O(3P0) and O2(b1Σg+) fragments produced by photolysis of ozone in the Huggins bands

Patrick O'Keeffe, Trevor Ridley, Kenneth P. Lawley, Robert R. J. Maier, and Robert J. Donovan

Citation: J. Chem. Phys. **110**, 10803 (1999); doi: 10.1063/1.479023
View online: http://dx.doi.org/10.1063/1.479023
View Table of Contents: http://jcp.aip.org/resource/1/JCPSA6/v110/i22
Published by the AIP Publishing LLC.

Kinetic energy analysis of $O(^3P_0)$ and $O_2(b\,^1\Sigma_g^+)$ fragments produced by photolysis of ozone in the Huggins bands

Patrick O'Keeffe, Trevor Ridley, Kenneth P. Lawley, Robert R. J. Maier, and Robert J. Donovan
Department of Chemistry, The University of Edinburgh, West Mains Road, Edinburgh EH9 3JJ, Scotland, United Kingdom

(Received 2 February 1999; accepted 11 March 1999)

The velocity profile of $O_2(b\,^1\Sigma_g^+, v=0)$ produced by photolysis of O_3 in the Huggins band region at 351.4 nm has been measured using a delayed pulsed field extraction time-of-flight technique confirming that this fragment is formed by single-photon absorption. The velocity profile of $O(^3P_0)$ produced by photolysis at 322.64 nm has also been obtained. $O(^3P_0)$ fragments are shown to be produced in coincidence with $O_2(X\,^3\Sigma_g^-)$, $O_2(a\,^1\Delta_g)$, and $O_2(b\,^1\Sigma_g^+)$. The relative contribution of each of these channels to the total $O(^3P_0)$ signal is reported and it is shown that spin-forbidden channels dominate the dissociation process at this wavelength. Two quite different primary crossings of the initially excited state are suggested to account for the change in the relative contribution of these three channels when photolysis is changed from resonance with a vibronic band of ozone to an off-resonance wavelength. The determination of the anisotropy parameter, $\beta(v)$, for these dissociation processes suggests that the transition dipole responsible for all of the Huggins band absorption has B_2 symmetry. © *1999 American Institute of Physics.* [S0021-9606(99)01121-6]

I. INTRODUCTION

Recent research into the photodissociation dynamics of ozone, O_3, following absorption in the Huggins band between 310 and 355 nm, has revealed that the dynamics is complex and still far from being fully understood.[1] The following channels are energetically accessible in this region:

(i) $O_3+h\nu(\lambda<310\,\text{nm})\rightarrow O(^1D)+O_2(a\,^1\Delta_g)$,
(ii) $O_3+h\nu(\lambda<411\,\text{nm})\rightarrow O(^1D)+O_2(X\,^3\Sigma_g^-)$,
(iii) $O_3+h\nu(\lambda<463\,\text{nm})\rightarrow O(^3P_J)+O_2(b\,^1\Sigma_g^+)$,
(iv) $O_3+h\nu(\lambda<612\,\text{nm})\rightarrow O(^3P_J)+O_2(a\,^1\Delta_g)$,
(v) $O_3+h\nu(\lambda<1180\,\text{nm})\rightarrow O(^3P_J)+O_2(X\,^3\Sigma_g^-)$.

Initially, it was thought that the spin-allowed channels, (A) and (E), accounted for the photodissociation products in the Huggins band: channel (A) can only occur in the Huggins system via hot band dissociation of O_3 which extends the threshold for this channel to 320 nm.[2] However, careful measurements of the quantum yield for $O(^1D)$ have shown that there is a wavelength independent yield which cannot be accounted for by the spin-allowed channel (A). Thus spin-forbidden dissociation, via channel (B), has been invoked to explain this observation.[1–10] Furthermore, Hancock *et al.*[11,12] have deduced that channel (D) is operative at these wavelengths from their analysis of time-of-flight (TOF) profiles of $O_2(a\,^1\Delta_g)$ fragments, detected by (2+1) resonance enhanced multiphoton ionization (REMPI) via the intermediate $d3s\sigma_g\,^1\Pi_g$ Rydberg state.

We have recently reported[13] the detection of $O_2(b\,^1\Sigma_g^+)$ fragments, following photolysis of O_3 in the (4,0,0), (3,1,0), (3,0,0), and (2,0,0) bands of the Huggins system. The production of $O_2(b\,^1\Sigma_g^+)$ was assigned to the spin-forbidden dissociation of O_3 via channel (C). The photofragment excitation (PHOFEX) spectrum of $O(^3P_0)$ fragments produced by the photolysis of O_3 over the wavelength range 335–345 nm was also recorded by scanning the photolysis laser wavelength while monitoring the yield of $O(^3P_0)$ via (2+1) REMPI. The observed excitation spectrum closely matched the Huggins band absorption features in O_3. In the work presented here we investigate the kinetic energy imparted to the fragments in order to gain a more detailed understanding of the dynamics and to provide confirmatory evidence for our earlier study. The kinetic energies of both $O_2(b\,^1\Sigma_g^+)$ and $O(^3P_0)$ have been measured in one- and two-color experiments, respectively.

II. EXPERIMENT

The two types of experiments which were performed in this work involved both one-color and two-color REMPI combined with kinetic energy release (KER) spectroscopy. The experimental setup for the two-color experiments consisted of a laser photolysis–laser probe method which used the outputs of two pulsed and independently tunable dye lasers (a Lambda Physik FL3002 and a Lambda Physik FL2002) pumped by a XeCl excimer laser (a Lambda Physik EMG 201 MSC). The laser setup for the one-color experiments simply utilized the same dye laser output both to dissociate O_3 and ionize the fragments. The wavelength region studied in the one-color experiments was generated by the fundamental output of DMQ whereas the two-laser experiments used the frequency doubled outputs of Rhodamine 101 and Coumarin 2. In the two-color arrangement, the counter-propagating pump and probe beams were focused to an overlapping point in a differentially pumped ionization chamber using lenses of focal length 6 cm and intersecting, at 90°, the

molecular beam of 5 Torr of O_3 in 1 atm of He. The production of the O_3 mixture was described in a previous communication.[13] The resulting ions were then collected by a linear time-of-flight mass spectrometer (TOF-MS) which could be operated in two modes.

(i) All REMPI spectra presented in this paper were recorded when the TOF-MS was operated in a dc mode. In this mode the ions were accelerated into the field-free drift region by a dc extraction field ($\sim$1260 $V\,cm^{-1}$) on the ionization chamber ion optics. In this mode there was no discrimination between fragments formed with different initial recoil velocities. The ion packet was then focused onto the microchannel plate detector by an Einzel lens. The resulting ion current was processed by a Stanford Research System SR250 boxcar integrator and recorded on a PC.

(ii) The KER experiments, on the other hand, required the TOF-MS to be operated in a pulsed mode where the fragments were allowed to separate spatially under the initial recoil velocities imparted to them by the photodissociation event. This separation was achieved by allowing the fragments to recoil under field-free conditions during a time delay, τ (typically 300 ns), between their formation by the laser pulse and acceleration by a pulsed field (risetime $<$50 ns). The time of flight of the resulting unfocused ions is related to the position of the ions in the extraction region when the field is applied, and therefore can be converted to the initial recoil velocities of the neutral fragments by solution of the time-of-flight equation. Parameters, such as the field gradient in the extraction region and laser focus position, required for the solution of this equation, were obtained by the calibration method described by Huang *et al.*[14] using the 225.65 nm photodissociation of O_2.[15] The recoil velocity of the atomic fragments formed in the photodissociation of O_2 is known and therefore can be substituted into the TOF equation for calibration.

Core-sampling collection conditions could be achieved by modifying a radial position sensitive detector of diameter 40 mm (usually sufficient to collect the entire ion packet). The central core of the ion packet can be selectively detected by reducing the active surface of the detector to a diameter of 8.5 mm, thus reducing the collection angle subtended by the detector from 4 to 0.87°. Also, the TOF profile could be recorded with the dissociation laser polarization either parallel or perpendicular to the detector axis. Rotation of the laser polarization was achieved by passing the beam through a Soleil Babinet prism.

III. RESULTS AND DISCUSSION

A. Kinetic energy analysis of $O_2(b\,^1\Sigma_g^+)$ fragments following photolysis of O_3 at 351.4 nm

In our earlier work we observed the formation of $O_2(b\,^1\Sigma_g^+)$ in the photolysis of O_3, using (2+1) REMPI via the $O_2(d3s\sigma_g\,^1\Pi_g \leftarrow\leftarrow b\,^1\Sigma_g^+)$ transition. This transition is observed in the region of 351.4 nm, and overlaps one of the bands in the Huggins system of O_3. It is therefore possible to measure the kinetic energy released to the $O_2(b\,^1\Sigma_g^+)$ fragment using a single laser and thus to check whether one-photon or two-photon absorption by O_3 is involved.[13] Figure 1(a) shows the yield of O_2^+ as a single laser is scanned through the 349.5–352.0 nm region. The main feature observed involves the overlap of the O-branch rotational lines, O(20) and O(22), of the (2,0) band of the $O_2(d3s\sigma_g\,^1\Pi_g \leftarrow\leftarrow b\,^1\Sigma_g^+)$ transition,[16] with an absorption band of ozone, which according to the assignments of Katayama,[17] corresponds to the (2,0,0) band of the Huggins system. The O(20) and O(22) rotational lines were observed with large intensities in the two-color $[(1+1')+1]$ REMPI excitation of the same vibronic band of $O_2(b\,^1\Sigma_g^+)$[13] produced by dissociation of O_3 with a photolysis laser wavelength fixed, coincident with a Huggins band absorption. The positions of the other

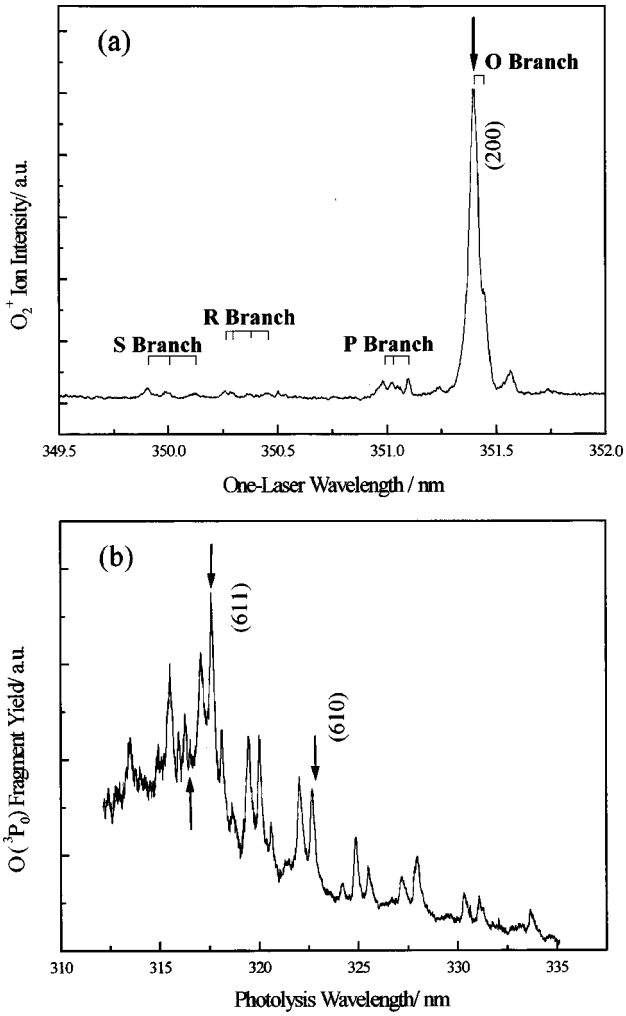

FIG. 1. (a) One-color REMPI spectrum of O_3 between 349.5 and 352 nm recorded by collecting O_2^+ ions. The ions are formed as a result of a coincidental energy overlap of the (2,0,0) Huggins band absorption in O_3 and a (2+1) REMPI transition involving $O_2(b\,^1\Sigma_g^+, v=0)$ fragments. (b) The PHOFEX spectrum for $O(^3P_0)$ fragment yield detected following photolysis of O_3 between 312 and 325 nm: the vibrational assignments of the absorption bands are taken from Ref. 17. The $O(^3P_0)$ fragments are detected by the $O(3p\,^3P_0 \leftarrow\leftarrow 2p\,^3P_0)$ (2+1) REMPI transition with a probe laser wavelength of 226.23 nm. The lowest arrow indicates the wavelength used for off-resonance photolysis (see text).

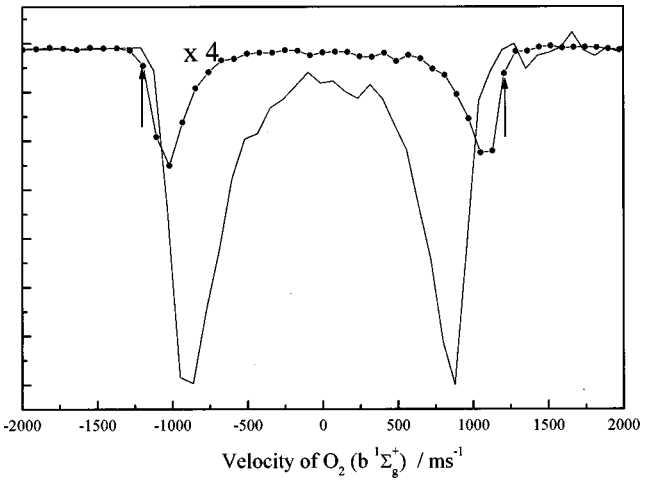

FIG. 2. The velocity release profiles of the $O_2(b\ ^1\Sigma_g^+, v=0, J=18-20)$ fragments produced by photolysis of O_3 at 351.4 nm and detected at the same wavelength by the O-branch of a $(2+1)$ REMPI transition via the $O_2(d3s\sigma_g\ ^1\Pi_g, v=2)$ intermediate state. The solid line is the full ion packet, whereas the closed circles show the profile $(x4)$ produced using the core-sampling method. A delay of 300 ns was used for the pulsed field extraction. The arrows indicate the velocities used in the kinetic energy release calculations.

limited number of rotational transitions are also indicated in Fig. 1(a). These transitions are only observed very weakly in the present one-color spectrum as the one-photon wavelengths at which they occur do not coincide with a Huggins band absorption in O_3.

The velocity release profiles shown in Fig. 2 were recorded by photolyzing O_3 and detecting the $O_2(b\ ^1\Sigma_g^+, v''=0, J''=20-22)$ fragments using linearly polarized light at 351.4 nm, indicated by the arrow in Fig. 1(a), with its electric field vector parallel to the TOF axis. The profiles were recorded by summing over 1000 laser shots and using a pulsed field delayed by 300 ns from the laser pulse. The center of mass (c.m.) frame recoil velocity can be determined by considering that the velocity measured in this experiment is not the actual velocity, v, but the projection of the recoil vector, v_z, onto the detection axis, z. However, the core-extracted velocity release profile (the closed circles in Fig. 2) involves the discrimination against any fragments with significant velocities in the plane perpendicular to the z axis and therefore the maximum velocities in this case correspond to the c.m. frame recoil velocity, i.e., $v_z \approx v = 1200 \pm 100\ ms^{-1}$ (indicated by arrows on Fig. 2). The velocity release profile for the full ion packet (the solid line in Fig. 2) is included for comparison and shows the effect of the core-sampling technique on the intensity and width of the profile.

Using this value of the c.m. frame velocity release to the O_2 fragment, the translational energy release, $\langle E_{\text{trans}}(\text{exp})\rangle$, from the dissociation process can be calculated as follows:

$$\langle E_{\text{trans}}(\text{exp})\rangle = \tfrac{1}{2} m_{O_2} v_{O_2}^2 + \tfrac{1}{2} m_O v_O^2 = \tfrac{3}{2} m_{O_2} v_{O_2}^2 = 5780 \pm 1000\ \text{cm}^{-1}. \quad (1)$$

This energy can be compared with the calculated translational energy, $\langle E_{\text{trans}}(\text{calc})\rangle$, for photodissociation processes involving the $O_2(b\ ^1\Sigma_g^+, v''=0, J''=20-22)$ fragment, from the equation

$$\langle E_{\text{trans}}(\text{calc})\rangle = nh\upsilon - \langle E_{\text{ass}}\rangle - \langle E_{\text{elec}}\rangle_{O_2} - \langle E_{\text{vib}}\rangle_{O_2} - \langle E_{\text{rot}}\rangle_{O_2} - \langle E_{\text{elec}}\rangle_O, \quad (2)$$

where n is the number of photons absorbed by O_3 prior to dissociation, $\langle E_{\text{diss}}\rangle$ is the energy threshold to forming the ground-state fragments,[2] $\langle E_{\text{elec}}\rangle O_2$, $\langle E_{\text{vib}}\rangle O_2$, and $\langle E_{\text{rot}}\rangle O_2$ are the electronic, vibrational, and rotational energies of the O_2 $(b\ ^1\Sigma_g^+,\ v''=0,\ J''=20-22)$, and $\langle E_{\text{elec}}\rangle O$ is the electronic energy of the atomic fragment. The effect of the rotation of the parent molecule is negligible due to the low rotational temperature of the beam. The resulting $\langle E_{\text{trans}}(\text{calc})\rangle$ for a one-photon photolysis producing the $O_2(b\ ^1\Sigma_g^+)$ fragment with $O(^3P_2)$ as the cofragment is $6200 \pm 80\ \text{cm}^{-1}$ [equivalent to an $O_2(b\ ^1\Sigma_g^+)$ velocity of $1240 \pm 8\ ms^{-1}$] compared with values of 890 ± 80, $18\,800 \pm 80$, and $34770 \pm 80\ \text{cm}^{-1}$ (470 ± 20, 2160 ± 5, and $2937 \pm 3\ ms^{-1}$) for two-photon processes with the $O(^1S_0)$, $O(^1D_2)$, and $O(^3P_2)$ cofragments, respectively. The quoted error in the $\langle E_{\text{trans}}(\text{calc})\rangle$ values is due to in part to the uncertainty of $\langle E_{\text{diss}}\rangle$ but mainly due to a separation of $\sim 120\ \text{cm}^{-1}$ between $J''=20$ and $J''=22$ of $O_2(b\ ^1\Sigma_g^+)$.[18] The true error will be slightly larger due to the approximations mentioned above. It is clear from these results that two-photon absorption can be eliminated from consideration and that the $O_2(b\ ^1\Sigma_g^+)$ fragments are produced solely via one-photon absorption followed by spin-forbidden dissociation of O_3. The experimentally measured translational energy of the channel, $\langle E_{\text{trans}}(\text{exp})\rangle$, matches the calculated values for this channel, $\langle E_{\text{trans}}(\text{calc})\rangle$, to well within experimental error.

B. Kinetic energy analysis of $O(^3P_0)$ fragments following photolysis of O_3

1. Identification of the cofragments

The spectrum shown in Fig. 1(b) is the PHOFEX spectrum of $O(^3P_0)$ fragments produced by the photolysis of O_3 over the wavelength range 312–335 nm. This spectrum was recorded by scanning the photolysis laser wavelength while monitoring the yield of $O(^3P_0)$ via the $O(3p\ ^3P_0 \leftarrow\leftarrow 2p\ ^3P_0)$, $(2+1)$ REMPI transition, with the probe laser tuned to 226.23 nm. The peaks correspond to vibronic bands of the Huggins system of O_3 and the relative intensities of the bands observed at $\lambda > 317$ nm are very similar to those observed in the absorption spectrum and quantified by Joens.[19] These vibronic bands were chosen for this experiment because their absorption cross sections are more than 50 times larger than the (2,0,0) band used in the one-color experiment.

The velocity release profiles shown in Figs. 3(b) and 3(c) are the core-sampled profiles of the $O(^3P_0)$ fragments recoiling from O_3 photolyzed at 322.64 nm, which correspond to the (6,1,0) band of Katayama's assignments,[17] recorded by summing over 3000 laser shots. Both profiles were recorded with the polarization of the probe perpendicular to the TOF axis, hence the $O(^3P_0)$ fragments resulting from photolysis

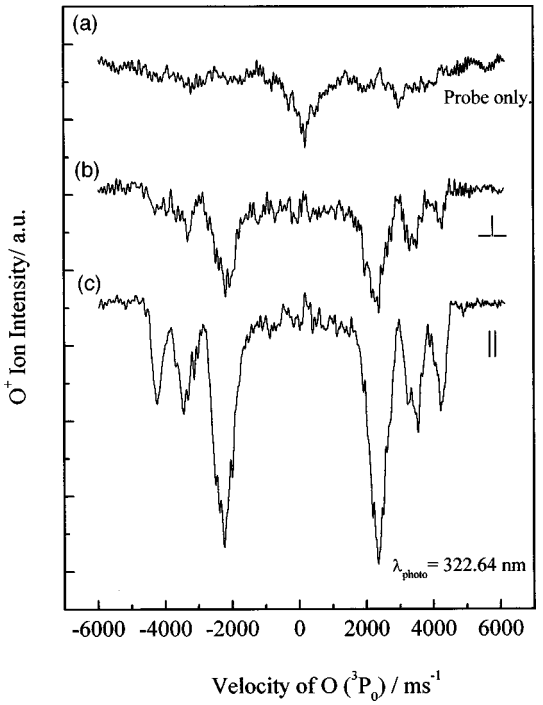

FIG. 3. The core-sampled velocity release profiles of the O($^3P_0$) fragments produced by photolysis of O_3. The signal due to the 226.23 nm probe laser alone which is polarized perpendicular to the TOF axis is shown in (a) (top) and forms a background signal which has already been subtracted from the profiles shown in (b) and (c). The profile in (b) was produced with the polarization of the 322.64 nm photolysis laser perpendicular to the TOF axis whereas that in (c) had the photolysis laser polarization parallel to the TOF axis.

of O_3 at the probe photon wavelength of 226.23 nm recoil predominantly perpendicular to the detection axis and therefore appear at velocity release ~ 0 ms^{-1}. The signal due to these O($^3P_0$) fragments, which is shown in Fig. 3(a), was recorded by averaging the signal of the probe laser only and comprises $<15\%$ of the total signal. This signal was then subtracted from the total profiles, resulting in those shown in Figs. 3(b) and 3(c) which are formed solely by dissociation of O_3 at 322.64 nm.

The profiles recorded with the polarization of the photolysis laser both perpendicular and parallel to the TOF axis show trimodal velocity distributions of O($^3P_0$) fragments with velocity peaks corresponding to 2380 ms^{-1} [full width at half maximum (FWHM) 600 ms^{-1}], 3430 ms^{-1} (FWHM $=500$ ms^{-1}), and 4225 ms^{-1} (FWHM$=370$ ms^{-1}). Based on the core-sampling approximation, the velocity release profiles of the O($^3P_0$) fragments can be converted to an internal energy distribution of the O_2 cofragments using a procedure described by Syage.[20] The resulting internal energy distribution of the O_2 fragments formed by the same photolysis events as O($^3P_0$), shown in Fig. 4, appears to show three essentially featureless peaks corresponding with vibrational/rotational distributions in $O_2(X\,^3\Sigma_g^-)$, $O_2(a\,^1\Delta_g)$, and $O_2(b\,^1\Sigma_g^+)$. Also, the possibility of a bimodal vibrational distribution in either the $O_2(X\,^3\Sigma_g^-)$ or the $O_2(a\,^1\Delta_g)$ fragments must be considered. It is known that a bimodal vibrational distribution in $O_2(X\,^3\Sigma_g^-)$ fragments is produced following 226 nm photolysis of O_3.[21] However, as the photolysis wavelength is increased to 266 nm, this bimodal distribution is lost.

The only method by which vibrational distributions of the molecular fragments can be determined with absolute certainty is by state-specific detection of each vibrational level of each molecular state. $O_2(X\,^3\Sigma_g^-)$ fragments have not been detected in this fashion as nascent products of Huggins band photolysis. However, the first peak in the internal energy distribution of Fig. 4, centered at 4000 cm^{-1}, must be due to dissociation to ground-state O_2 as it is below the term energy of the first excited state, $O_2(a\,^1\Delta_g)$. Also, Denzer *et al.*[10] have reported the detection of $O_2(a\,^1\Delta_g)$ fragments in unassigned rotational levels following photolysis in the 320–322 nm region and have shown by kinetic energy analysis of these fragments that spin-forbidden photolysis via channel (D) is partly responsible for production of these fragments. Using similar techniques, they have also reported

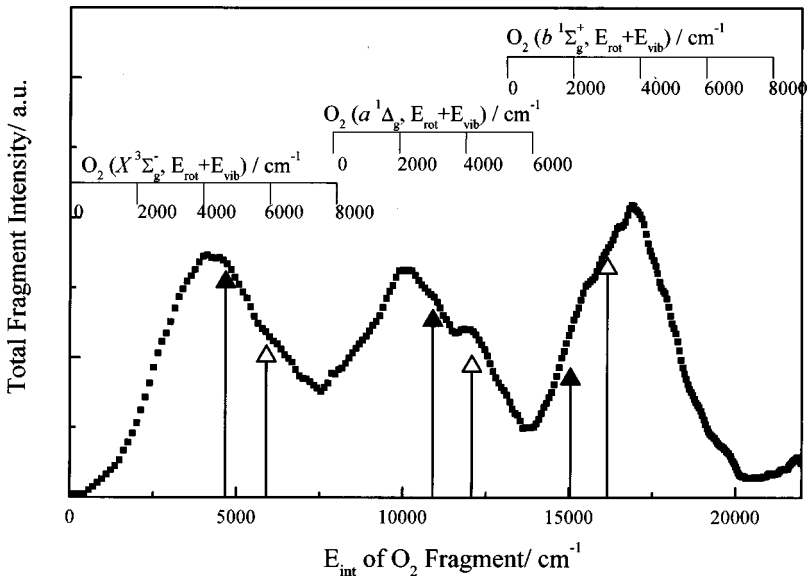

FIG. 4. The internal energy distribution of O_2 fragments formed in the same photolysis events as O($^3P_0$) fragments produced by the photolysis of O_3 at 322.64 nm. The ladders indicate the amount of energy above the zero-point energies of the $O_2(X\,^3\Sigma_g^-)$, $O_2(a\,^1\Delta_g)$, and $O_2(b\,^1\Sigma_g^+)$ fragments. The closed and open arrows indicate the most probable value in the rotational energy distribution of the molecular fragment $\langle E_{rot}\rangle_{O_2}$ calculated using a simple impulsive model of dissociation (see text for details) for $v=0$ and 1, respectively, for each of the states.

the spin-forbidden production of $O_2(a\,^1\Delta_g, v=1, J=28)$ fragments by photolysis of O_3 at 327.93 nm. Therefore, it seems that rotationally excited O_2 ($a\,^1\Delta_g$, $v=0$ and 1) fragments are produced by photolysis in the Huggins bands and probably account for the second peak in Fig. 4, centered at 10 000 cm^{-1}. In a previous report[13] we have communicated the spectroscopic detection of $O_2(b\,^1\Sigma_g^+, v=0)$ from the spin-forbidden photolysis at four wavelengths between 335 and 352 nm. Analysis of our spectra reveals that these fragments are produced in high rotational levels with a distribution centered around $J=35$ for photolysis at 337.2 nm.[16] The TOF profile of the $O(^3P_0)$ fragment recorded at this photolysis wavelength contains two peaks. The most intense peak appears with a similar velocity as the slowest peak in Fig. 3(c) and is attributed to the $O_2(b\,^1\Sigma_g^+)$ state cofragment, the second is attributed to the unresolved combination of $O_2(X\,^3\Sigma_g^-)$ and $O_2(a\,^1\Delta_g)$ state cofragments. Therefore, it is concluded that the lowest velocity peak in Fig. 3 (c), centered around 2380 ms^{-1}, is due to the photolysis of O_3 via channel (C), i.e., to yield $O(^3P_0)$ and $O_2(b\,^1\Sigma_g^+)$.

2. The nature of the dissociation processes

The detection of O_2 fragments in low vibrational levels but with large rotational excitation suggests that a simple impulsive model for dissociation may reproduce the experimental distributions. The assumptions required for this model are that the dissociation takes place on a very steeply repulsive potential and that the recoil vector lies along the dissociating bond. A particularly straightforward implementation of this model, described by Levene and Valentini,[22] can be used to predict the most probable value in the rotational energy distribution of each vibrational level of the molecular, $\langle E_{\mathrm{rot}}\rangle_{O_2}$, using the formula

$$\langle E_{\mathrm{rot}}\rangle_{O_2} = \frac{\langle E_{\mathrm{avl}}\rangle \sin^2\theta}{4-\cos^2\theta}, \tag{3}$$

where $\langle E_{\mathrm{avl}}\rangle = \langle E_{\mathrm{trans}}\rangle + \langle E_{\mathrm{rot}}\rangle$ and θ is the bond angle of the molecule in the dissociating state, which is assumed to be the same as that of the ground state in the present calculation. The $\langle E_{\mathrm{rot}}\rangle_{O_2}$ of $O_2(X\,^3\Sigma_g^-, v=0,1)$, $O_2(a\,^1\Delta_g, v=0,1)$, and $O_2(b\,^1\Sigma_g^+, v=0,1)$ were calculated using (3) and are illustrated in increasing energy by the arrows in Fig. 4. The qualitative matching of the results of this model with those of the experiment support the assignment of the three peaks made previously. However, there are small but real deviations of the experimental results from this impulsive model, which predicts slightly more rotational energy in the $O_2(X\,^3\Sigma_g^-)$ and $O_2(a\,^1\Delta_g)$ states, but less than observed in the $O_2(b\,^1\Sigma_g^+)$, as illustrated by the positions of the two arrows relative to the maximum of each of the three peaks. This suggests that at least two significantly different dissociation paths exist.

The raw TOF profiles in Fig. 5 illustrate the comparison between photolysis of O_3 in discrete vibronic bands and in the continuum between them. The profiles in Figs. 5(b) and 5(c) were recorded with photolysis wavelengths of 316.64 nm (off-resonance) and 317.64 nm (resonant), respectively, as indicated by arrows in Fig. 1(b). The polarization of the probe laser is again perpendicular to the TOF axis in both cases and the arrival times of the fragments produced by the probe laser alone are shown for comparison in Fig. 5(a). The lower resolution of these profiles compared to those in Fig. 3 is due to the fact that only partial core-sampling conditions are operative in this experiment and therefore direct extraction of the speed distribution or angular information is not possible. However, this has the advantage that more of the ion packet is detected and therefore there is a much larger signal allowing comparison with the weaker off-resonance signal.

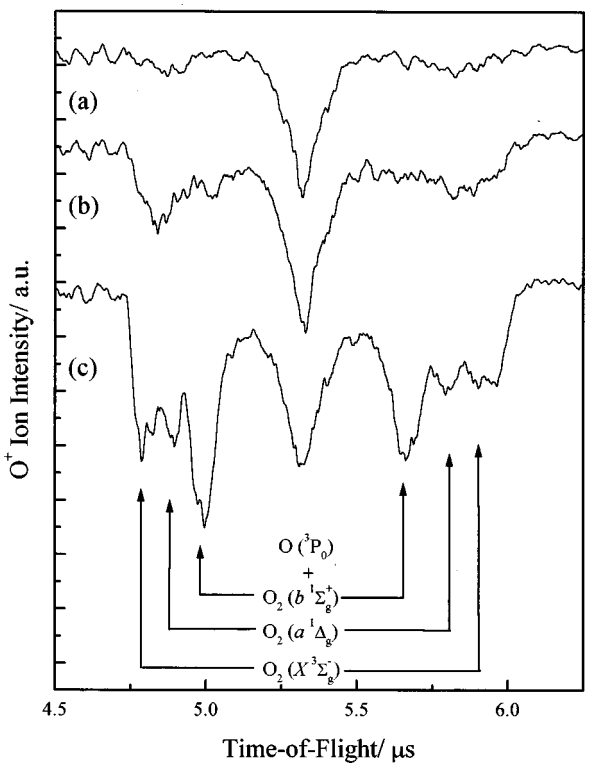

FIG. 5. The TOF profiles of $O(^3P_0)$ fragments produced from photolysis of O_3 at various wavelenths, detected via (2+1) REMPI using radiation of wavelength. (a) 226.23 nm; (b) 316.64 nm, i.e., not resonant with a discrete absorption band; (c) 317.64 nm, i.e., resonant with a discrete absorption band of O_3.

The main point illustrated in Fig. 5 is that while the peak assigned to the production of $O(^3P_0)$ in coincidence with $O_2(b\,^1\Sigma_g^+)$ is the most intense when the photolysis wavelength is resonant with a discrete vibronic band, this channel is barely detectable for off-resonance (continuum) dissociation. The $O(^1D)+O_2(X\,^3\Sigma_g^-)$ and $O(^3P_J)+O_2(a\,^1\Delta_g)$ products are believed to be formed predominantly as a result of the crossing of the singlet exit channel, which produces $O(^3P_J)+O_2(X\,^3\Sigma_g^-)$, by repulsive triplet states correlating with these products.[6] If a third crossing in the same initial exit channel were responsible for the observation of $O(^3P_J)+O_2(b\,^1\Sigma_g^+)$, the ratios of $X{:}a{:}b$ observed when the photolysis photon is resonant with a discrete absorption band should be very similar to those when it is off resonance. The simplest explanation would seem to be that the predissociation of the bound levels of the $^1B_2$ state occurs via a primary spin-forbidden crossing to a surface that correlates directly

TABLE I. Observed $\beta(v)$ parameters for the three velocity ranges of the peaks observed in the velocity release profiles of $O(^3P_0)$ produced by the photolysis of O_3 at 322.64 nm which are shown in Fig. 3, the channel assignments, and the percentage contributions of each of these channels to the overall $O(^3P_0)$ signal at this wavelength.

Velocity peak±FWHM ms^{-1}	$\beta(v)$	% of total $O(^3P_0)$ signal	Channel assignment
2380±600	0.6±0.1	34	$O(^3P_0)+O_2(b\,^1\Sigma_g^+)$
3430±500	0.6±0.3	35	$O(^3P_0)+O_2(a\,^1\Delta_g)$
4225±370	0.6±0.3	31	$O(^3P_0)+O_2(X\,^3\Sigma_g^-)$

with channel (C), $O(^3P_J)+O_2(b\,^1\Sigma_g^+)$. This is quite separate from the spin-allowed crossing that leads to rapid predissociation and has been suggested to indirectly feed channels (B) and (D).[6] This switch in initial crossing may account for the different deviations from the simple impulsive model observed in channel (C) when compared with channels B and D.

3. The relative contributions of the $O_2(X\,^3\Sigma_g^-)$, $O_2(a\,^1\Delta_g)$, and $O_2(b\,^1\Sigma_g^+)$ cofragments to the $O(^3P_0)$ yield at 322.64 nm

The relative contributions of the three channels to the total $O(^3P_0)$ signal at 322.64 nm were estimated from the areas of the peaks in Fig. 4 and are shown in Table I. The fact that when the photolysis wavelength is resonant with a discrete vibronic band, the percentages of each of the three cofragments are very similar, indicates that the channels which yield $O_2(a\,^1\Delta_g)$ and $O_2(b\,^1\Sigma_g^+)$ are important in spite of their spin-forbidden nature.

This observation has some implications for the field of atmospheric modeling where, in general, the dissociation channel which produces $O(^3P_J)+O_2(b\,^1\Sigma_g^+)$ has been ignored. The molecular O_2 yields described in this paper are specific to photolysis following absorption into one particular vibronic band and only in combination with $O(^3P_0)$. Further work is being carried out to extend these studies to examine the O_2 product distributions as a function of the vibronic states excited in O_3. The percentage of each of the $O(^3P_J)$ multiplets will be monitored as a function of photolysis wavelength.

4. Measurement of the anisotropy parameter, β(v)

Information on the angular distribution of the fragments can also be extracted from the fully core-extracted profiles in Fig. 4 as the correlation between the recoil vector, **v**, of the products and the electric field vector of the dissociating light, **E**, is described for a one-photon photolysis process by[23]

$$I(\theta)=\frac{\sigma}{4\pi}[(1+\beta(v)P_2(\cos\theta))], \tag{4}$$

where θ is the angle of recoil relative to the electric field vector of the dissociating light, P_2 is the second-order Legendre polynomial, and $\beta(v)$ is an anisotropy parameter which gives a measure of the anisotropy of the dissociation. The anisotropy parameters, $\beta(v)$, can be calculated under core-sampling conditions[20] using the formula

$$\beta(v)=\frac{I_0(v)-I_{90}(v)}{\frac{1}{2}I_0(v)+I_{90}(v)}, \tag{5}$$

where $I_0(v)$ is the area under the Gaussian fit to each of the peaks in the $E_{photo}\|$TOF axis profile and similarly $I_{90}(v)$ is extracted from the $\mathbf{E}_{photo}\perp$ TOF axis profile. The polarization of the probe laser will not cause any preferential detection of $O(^3P_0)$ fragments as no $\mathbf{E}-\mu-\mathbf{J}$ vector correlation is possible. Thus the anisotropy observed in the ion packet is a result of the dissociation process alone. The calculated $\beta(v)$ parameters are shown in Table I where the larger error for the faster fragments is due to the difficulty in measuring the $I_{90}(v)$ due to the lower intensity for the $\mathbf{E}_{photo}\perp$ TOF axis profile shown in Fig. 3.

There is still controversy as to whether the electronic transition responsible for the Huggins bands is to the $2\,^1A_1$ state or to the $1\,^1B_2$ state (responsible for the more intense Hartley band). $\beta(v)$ should provide some information about the orientation of the transition moment and therefore which of these excitation processes is more likely. For a vibronic transition to a $^1A_1$ state, with $\Delta v_3=$ even, the transition moment is parallel to the C_2 axis, whereas for a transition to a $^1B_2$ state, with $\Delta v_3=$ even, the transition moment is perpendicular to the C_2 axis and in the plane of the molecule. Therefore, the limiting value of $\beta(v)$ for excitation to an excited state of $^1A_1$ symmetry followed by instantaneous dissociation in the ground-state geometry, with the fragments recoiling along the direction of the bond being broken, is -0.18, which compares with a value of 1.18 obtained from a similar calculation for an excited state of $^1B_2$ symmetry. The observed value of $\beta(v)$ can differ from these limiting values as a result of processes which make the distribution more isotropic. For example, the rotation of the parent molecule may couple directly with the recoil vectors of the fragments or the dissociating molecule may rotate while dissociating, a process which depends on the lifetimes of the excited state.[24] However, there is also the possibility of a geometry change in the excited state which can make the angular distribution either more or less anisotropic. The experimental value is an intermediate between the two limiting values and so does not conclusively identify the symmetry of the excited state. Nevertheless, it is possible to conclude that to reproduce the observed $\beta(v)$ value, the geometry of the state involved in a $^1A_1(\Delta v_3=$ even) transition would be required to change from the ground-state bond angle of 116.8 to $<90°$.

IV. CONCLUSION

The velocity release profile of the $O_2(b\,^1\Sigma_g^+)$ fragments formed from photolysis of O_3 at 351.4 nm has been measured and it is has been shown conclusively that these fragments are produced via one-photon spin-forbidden dissociation of O_3 in the Huggins band via $O_3+h\nu\rightarrow O(^3P_J)+O_2(b\,^1\Sigma_g^+)$.

The velocity release profile of the $O(^3P_0)$ fragments was also measured and analyzed to reveal that O_3 dissociates following absorption of one photon at 322.64 nm to give $O(^3P_0)+O_2(X\,^3\Sigma_g^-)$, $O(^3P_0)+O_2(a\,^1\Delta_g)$, and $O(^3P_0)+O_2(b\,^1\Sigma_g^+)$ products. At this wavelength, which is resonant with a discrete vibronic band in the Huggins system, a

conversion to the energy distribution of the O_2 cofragments shows that dissociation via spin-forbidden triplet channels accounts for approximately two-thirds of the $O(^3P_0)$ fragments. This energy distribution is very different when the photolysis photon is off-resonance, indicating that two quite different dissociation processes are taking place. The determination of the anisotropy parameter, $\beta(v)$, suggests that the transition responsible for the Huggins band absorption has B_2 symmetry.

ACKNOWLEDGMENTS

P.O.K. wishes to thank the University of Edinburgh for financial support.

[1] A. R. Ravishankara, G. Hancock, M. Kawasaki, and Y. Matsumi, Science **280**, 60 (1998).
[2] K. Takahashi, M. Kishigami, N. Taniguchi, Y. Matsumi, and M. Kawasaki, J. Chem. Phys. **106**, 6390 (1997).
[3] R. K. Talukdar, C. A. Longfellow, M. K. Gilles, and A. R. Ravishankara, Geophys. Res. Lett. **25**, 143 (1998).
[4] E. Silvente, R. C. Richter, M. Zheng, E. S. Saltzmann, and A. J. Hynes, Chem. Phys. Lett. **264**, 309 (1997).
[5] K. Takahashi, M. Kishigami, Y. Matsumi, M. Kawasaki, and A. J. Orr-Ewing, J. Chem. Phys. **105**, 5290 (1996).
[6] K. Takahashi, N. Taniguchi, Y. Matsumi, M. Kawasaki, and M. N. R. Ashfold, J. Chem. Phys. **108**, 7161 (1998).
[7] K. Takahashi, Y. Matsumi, and M. Kawasaki, J. Phys. Chem. **100**, 4084 (1996).
[8] W. Armerding, F. J. Comes, and B. Schulke, J. Phys. Chem. **99**, 3137 (1995).
[9] S. M. Ball, G. Hancock, S. E. Martin, and J. C. Pinot de Moira, Chem. Phys. Lett. **264**, 531 (1997).
[10] W. Denzer, G. Hancock, J. C. Pinot de Moira, and P. Tyley, Chem. Phys. **231**, 109 (1998).
[11] S. M. Ball, G. Hancock, J. C. Pinot de Moira, C. M. Sadowski, and F. Winterbottom, Chem. Phys. Lett. **245**, 1 (1995).
[12] S. M. Ball, G. Hancock, and F. Winterbottom, Faraday Discuss. **100**, 215 (1995).
[13] P. O'Keeffe, T. Ridley, S. Wang, K. P. Lawley, and R. J. Donovan, Chem. Phys. Lett. **298**, 368 (1998).
[14] H. J. Huang, J. Griffiths, and M. A. El-Sayed, Int. J. Mass Spectrom. Ion Processes **131**, 265 (1994).
[15] B. Buijsse, W. v. d. Zande, B. Lewis, A. Eppink, and D. H. Parker, J. Chem. Phys. **108**, 7229 (1998).
[16] B. R. Lewis, M. L. Ginter, and J. Morril (private communication).
[17] D. H. Katayama, J. Chem. Phys. **71**, 815 (1979).
[18] T. G. Slanger and P. C. Cosby, J. Phys. Chem. **92**, 267 (1988).
[19] J. A. Joens, J. Chem. Phys. **101**, 5431 (1994).
[20] J. A. Syage, J. Chem. Phys. **105**, 1007 (1996).
[21] R. J. Wilson, J. A. Mueller, and P. L. Houston, J. Phys. Chem. A **101**, 7593 (1997).
[22] H. B. Levene and J. J. Valentini, J. Chem. Phys. **87**, 2594 (1987).
[23] R. N. Zare, Mol. Photochem. **4**, 1 (1972).
[24] G. E. Busch and K. R. Wilson, J. Chem. Phys. **56**, 3638 (1972).